Nonlinear Mechanooptical Behavior of Uniaxially Stretched Poly(lactic acid): Dynamic Phase Behavior

Jake Mulligan and Miko Cakmak*

Polymer Engineering Department, The University of Akron, Akron, Ohio 44325-0301

Received June 17, 2004; Revised Manuscript Received December 17, 2004

ABSTRACT: The mechanooptical behavior of melt-cast amorphous poly(L-lactic acid) (PLA) films in the rubbery state was investigated using an apparatus that allows for direct measurement of true stress, true strain, and birefringence in real time under well-controlled temperature over a wide range of stretching rates. Three distinct regimes of stress−optical behavior are observed during uniaxial deformation of PLA films in the rubbery state. Regime I deformation is characterized by adherence to the stress optical rule; within this regime, birefringence remains linearly proportional to stress with a stress optical constant of 3.1 GPa^{-1}. This is followed by either a positive deviation from linearity into regime II at higher temperature and/or lower rates or a negative deviation into regime IIIa at lower temperatures and/or higher rates. Films exhibiting regime II behavior eventually deviate into regime IIIc behavior at higher levels of deformation. The appearance of regime II is associated with strain-induced crystallization. In the absence of regime II behavior, the polymer remains uncrystallized, yet becomes highly oriented, exhibiting "nematic-like" order. This stable nematic-like order prevails at all large deformation levels with no sign of crystallization. When nematic-like order is present, the strain optical behavior was found to exhibit linear or near-linear behavior in a wide deformation range. Conversely, this behavior is nonlinear with the development of strain-induced crystallization. On the basis of the structural and true mechanical measurements, a dynamic phase diagram was constructed for defining the structure development during the rubbery state uniaxial deformation of PLA.

Introduction

In the past, the use of poly(lactic acid) (PLA) has been limited to specialty biomedical applications[1,2] due to the high cost of production of the lactide monomer precursor that is necessary in the production of PLA. With the recent advent of better production techniques,[3] PLA is becoming economically viable. This polymer is bioresorbable, and this property coupled with its attractive physical, mechanical, and optical properties make it a good alternative to many currently used commodity polymers including PET and polypropylene.

PLA is a slow crystallizing polymer, and under normal processing conditions, it can be quenched into the glassy state. This is one of the biggest advantages of these polymers belonging to the general class of slow crystallizing polymers that include poly(ethylene terephthalate),[4] poly(ethylene naphthlate),[5−7] poly(lactic acid),[8] and poly(phenylene sulfide).[9,10] After being quenched into the amorphous state, films produced from slow crystallizing polymers can be reheated to the rubbery state between their glass transition and cold crystallization temperatures and can be stretched without the complicating effects of preexisting crystallites.

Previous studies have shown that there is a significant relationship between mechanical stimulus and birefringence. The stress optical rule (SOR) has been used extensively in polymer melts and was also shown to be valid for amorphous polymers at low to moderate stress levels[11,12]

$$\Delta n = C\sigma$$

where Δn is the birefringence, C is the stress optical constant, and σ is the true stress. However, beyond low to moderate stress levels or during phase changes (such as crystallization), deviations from the linear SOR have been observed. If strain-induced crystallization occurs, a positive deviation from linearity occurs.[13−15] Even noncrystallizable polymers may show deviation from SOR linearity.[16] Near their glass transition temperature, noncrystallizing polymers may initially exhibit photoelastic glassy behavior with stress increasing rapidly while birefringence increases slowly.[16−23] Furthermore, amorphous polymers that do not show this initial photoelastic glassy behavior may show negative deviation from SOR at higher levels of stress. This has been attributed to the non-Gaussian segmental distribution achieved when the chains approach their finite extensibility.[16,24−26] While this negative deviation has been shown to occur experimentally for noncrystallizable polymers,[16,12,27,28] it has not been reported for the strain crystallizable polymers.

Clearly, an understanding of the effects of processing parameters on stress optical relationships during deformation can provide a means of controlling material properties through control of orientation and phase development. The majority of the on-line studies on the phase development during deformation have focused on PET.[4,29−31] SAXS studies have indicated that a transient smectic order exists prior to crystallization at high rates and low temperatures, indicating that while the chains are highly oriented, they may not crystallize.[29−31] It is, however, difficult to capture PET in such a state as crystallization occurs immediately following the development of this transient phase presumably due to the rapidity of chain motions in PET caused by its relatively low molecular weight. Beyond the inability to capture and freeze PET in such a state, extremely high strain rates were employed in order to attain the transient smectic phase. These extremely high deformation rates lead to rapid plastic heating during stretching, further

* Corresponding author: e-mail Cakmak@uakron.edu.

10.1021/ma048794f CCC: $30.25
Published on Web 02/09/2005

complicating the observed phenomenon by heating the material into the temperature range in which the rate of thermal crystallization becomes significant. The synchrotron X-ray studies utilized in these past studies do not adequately clarify the physical changes in the early stages of structural evolution from the amorphous rubbery state to the oriented crystalline state. Birefringence technique provides a rapid and quantifiable measure of the overall anisotropy of the polymer chains undergoing these changes under rapid deformation rates from amorphous precursors. This is essential to quantitatively understand the critical conditions under which the structural formation mechanisms of the material are altered.

Our preliminary studies on birefringence development during the uniaxial deformation of PLA have indicated that two possible structures may form during stretching: (i) an orientation-induced crystallized PLA and (ii) a "nematic-like" phase of highly oriented chains.[32−35] The advantage of PLA as a model material was shown in these limited studies. While PLA is a slow crystallizing polyester that possesses rubbery state deformability and strain crystallization characteristics similar to PET, it can be obtained in much higher molecular weights (up to $\sim 1 \times 10^6$) than PET (up to 5×10^5). This leads to the presence of much higher entanglement densities in PLA, which suppresses the orientation relaxation mechanisms during the rubbery state deformation. This allows the chains to be easily frozen with minimal alteration of the overall structure developed up to a specified deformed state. These characteristics allow an in-depth study of these transient structures by off-line techniques even when there are minor changes that occur when transporting the deformed samples to the off-line measurement devices.

This paper presents a comprehensive on-line birefringence−true stress and true mechanical study of the deformation of PLA in the rubbery state from amorphous precursors over a wide range of rates and temperatures.

Experimental Section

Materials and Film Preparation. Cargill Dow, LLC, provided the Natureworks 4043D PLA (with a D-isomer content of approximately 2%) that was used for this study. The molecular weight of the PLA was provided by the company and was measured by GPC while using polystyrene standards. The number-average molecular weight (M_N) was ca. 130 000 g/mol, and the weight-average molecular weight (M_W) was ca. 150 000 g/mol. Immediately before processing, the PLA pellets were dried under a vacuum of 35 in.Hg at 80 °C for 24 h. The extrusion film casting was performed with a Prodex $1^1/_2$ in. single screw extruder, equipped with a polyester specific screw. The chill roll temperature was kept at 36 °C, and the chill roll was placed approximately $^1/_3$ in. below the die exit. The temperatures in zones 1−3 of the extruder were set to 156, 180, and 190 °C, and the die temperature was set at 190 °C. The die used was coat-hanger-shaped, with its divergence forming an angle of 120° and measuring 12 in. across at the outlet. The temperature inside the die lip was verified with a hand-held thermocouple, and the temperature at the very beginning of film processing varied 7−10 °C from either side of the die to the center. After the melt passed through the die for a short time, the temperature at the die lip became even across the die lip and remained at approximately 190 °C. Under these conditions, we produced cast amorphous films of about 250 μm thickness. These cast films were found to be amorphous and unoriented using DSC and birefringence techniques.

Stress−Strain Behavior with On-Line Birefringence. The dumbbell-shaped samples were cut from the cast film to a width of 48.5 mm and a length of 34.5 mm between the machine's clamps. The on-line mechanooptical instrumentation designed by our group, and used for this study, is described in greater detail in previous literature.[36] After preconditioning the samples at the desired temperature for at least 10 min, they were stretched at rates of 60 (0.01) (0.325), 120 (0.02) (0.65), 240 (0.04) (1.3), 480 (0.08) (2.6), and 960 (0.16) (5.2) %/min (s^{-1}) (mm/s). The stretching temperatures ranged from 60 to 95 °C, where the material remains in the rubbery state, and thermally activated crystallization rates remain insignificant.

DSC Measurements. A TA Instruments Q1000 DSC was used for the off-line DSC study. Samples of approximately 12 mg were crimped in aluminum pans and were then scanned with a heating rate of 20 °C/min under a dry nitrogen blanket. The TA Thermal Analysis software was used for analyzing the DSC results. The crystallinities were determined by subtracting the area under the cold crystallization peak (if present) from that of the melting endotherm and dividing by the heat of fusion of 100% crystalline PLA. The heat of fusion used for 100% crystalline PLA was 93 J/g.[37]

WAXD Measurements. The WAXD experiments utilized in this study were performed with a Bruker AXS D8 Discover General Area Detector Diffraction System, and its companion software was used for the WAXD measurement and analysis. Monochromatized Cu Kα ($\lambda = 1.54$ Å) radiation was used for all experiments. The sample-to-detector distance used was 12 cm, and the sample stage was set to capture one unique quadrant of the WAXD pattern. The generator settings were 40 kV and 40 mA. The crystalline orientation for selected planes was determined by taking an azimuthal scan through the diffraction angle corresponding to the plane of interest and subtracting this curve from a diffraction angle covering only the background:

$$I(\chi, \text{background subtracted}) = I(\chi, 2\theta_{\text{peak}}) - A^* I(\chi, 2\theta - \Delta)$$

where Δ is chosen sufficiently away from the diffraction plane to obtain the background information. The correction factor was determined at the azimuth where no crystalline diffraction is visible (~65°):

$$I(\text{corrected}) = I(65, 2\theta \text{ peak})/I(65, 2\theta - \Delta)$$

$$\langle \cos^2 \chi_{hkl} \rangle = \frac{\int_0^{\pi} I(\chi, \text{corrected}) \cos^2 \chi \sin \chi \, d\chi}{\int_0^{\pi} I(\chi, \text{corrected}) \sin \chi \, d\chi}$$

$$f_{hkl} = [3\langle \cos^2 \chi_{hkl} \rangle - 1]/2$$

where the *hkl* used was (200), I is the intensity, χ is the azimuthal angle, and f is the orientation factor.

Results and Discussion

As illustrated in Figure 1, the cast film exhibits the glass transition temperature at 60 °C, and it is in the rubbery state in a wide temperature range between 60 and 95 °C. Within the rubbery state, the thermal crystallization rates are quite slow, primarily due to high viscosity, allowing the polymer to be stretched while the thermal crystallization remaining highly suppressed. The areas under the cold crystallization and melting peaks are about the same, indicating that the original sample prior to scanning was essentially amorphous.

The stretching instrument, described in detail elsewhere,[36] provides real-time data on the optical retardation, thickness (and hence birefringence), cross-sectional area, and force on the sample while it is stretched continuously over a wide range of stretching speeds.

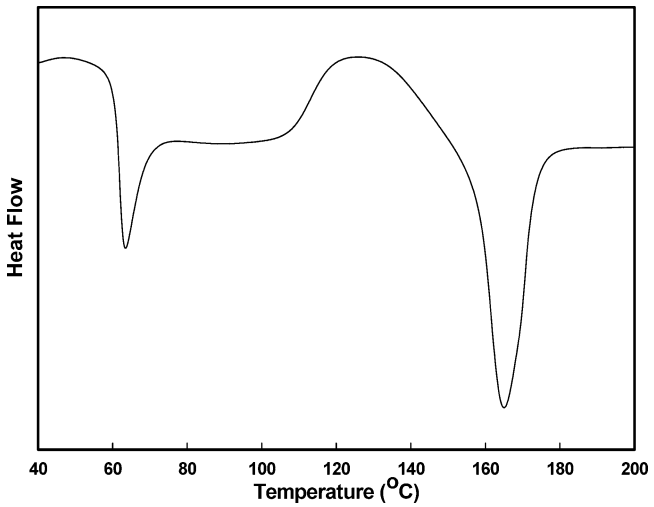

Figure 1. DSC scan of the as-cast PLA film.

This allows us to investigate the coupled relationships between birefringence−true stress and true stress−true strain at selected rates in the "rubbery state" window.

Figure 2a−c shows the true stress−true strain behavior of films stretched at varying temperatures and at rates 60, 240, and 960%/min for all the stretching temperatures investigated. This true mechanical behavior represents the real mechanical behavior at the stationary midpoint of the sample where the retardation and thickness measurements are continuously monitored.

When uniaxially stretched, PLA first exhibits a rubbery plateau, with higher temperatures and lower rates resulting in lower plateau stresses. At the end of the rubbery plateau, a rapid rise in stress signifies the hardening; this is exhibited at all temperatures and rates investigated. Higher rates and lower temperatures tend to lead to lower critical strains at which the strain hardening takes place. At very high temperatures or very low rates, this tendency is altered; this is most likely due to the increased role of thermally activated crystallization in effecting the deformation behavior. An example of this reversal in the strain hardening behavior can be seen during stretching at 960%/min and 76, 78, and 85 °C. Clearly, the 76 °C stretching results in the arresting of deformation at the midpoint of the sample at lower strains. This is a direct result of the strain hardening that occurs at these lower strains, enabling these regions to sustain higher stresses, and in turn allowing other parts of the sample to deform. The increase of temperature to 78 °C decreases this strain hardenability, resulting in the expected larger deformations at the point of measurement. However, this is not the case when the temperature is increased further to 85 °C where the onset of strain hardening is shifted to a lower true strain; this is most likely a result of the increased role of thermal crystallization during the course of stretching, particularly at slower deformation rates.

In each of the birefringence−true stress curves that are shown in Figure 3a−c for all three stretching rates 60, 240, and 960%/min, there is an initial linear stress optical rule regime exhibited by PLA films showing rubber-like mechanical behavior. During this "regime I" stress optical rule behavior of PLA, all of the birefringence vs true stress plots show a linear slope of 3.1 GPa^{-1} regardless of temperature or rate. As the deformation proceeds, deviation from the regime I linearity occurs. The nature and the location of this deviation are dependent on the deformation conditions. Higher temperatures and lower rates favor a positive deviation from linearity. This positive deviation occurs at lower stress levels as the temperature is increased or stretching rate is decreased as quantitatively shown in Figure 4. The critical birefringence values at negative deviation increase with increasing temperature, while the critical birefringence values at positive deviation into regime

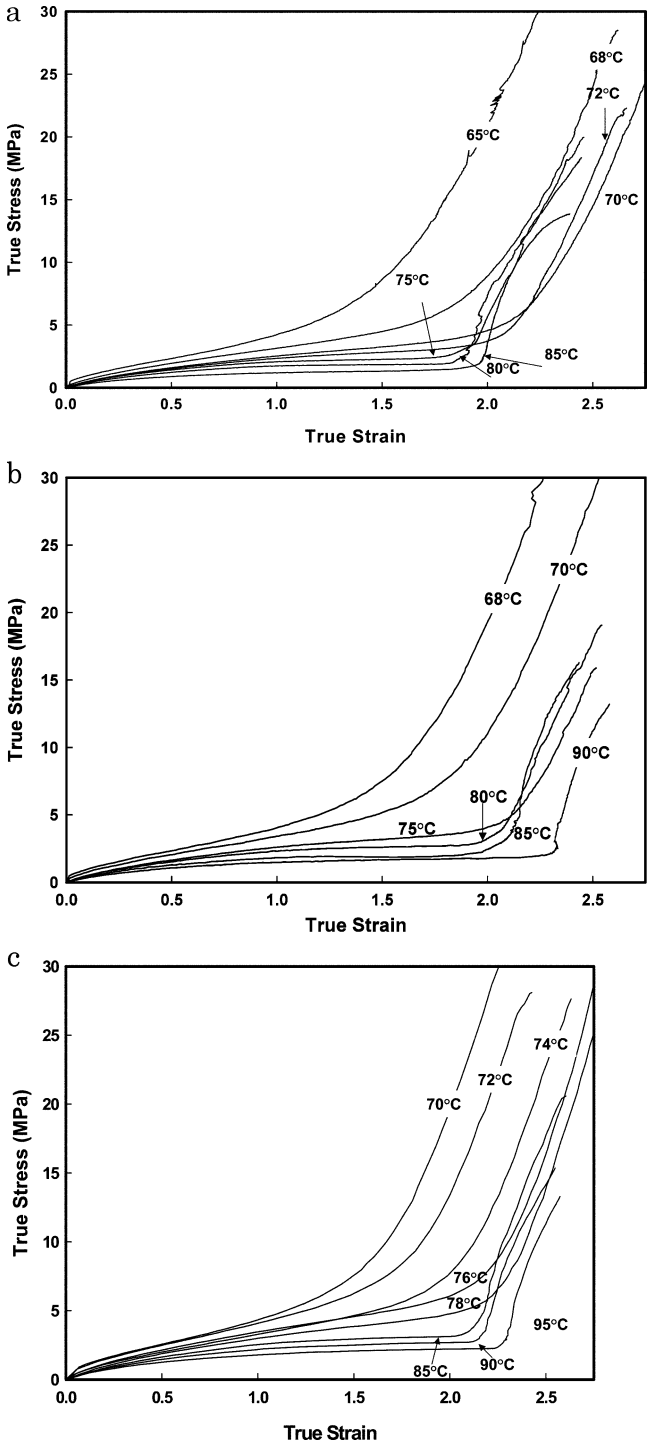

Figure 2. (a) True stress−true strain plots for PLA films stretched at 60%/min at various temperatures. (b) True stress−true strain plots for PLA films stretched at 240%/min at various temperatures. (c) True stress−true strain plots for PLA films stretched at 960%/min at various temperatures.

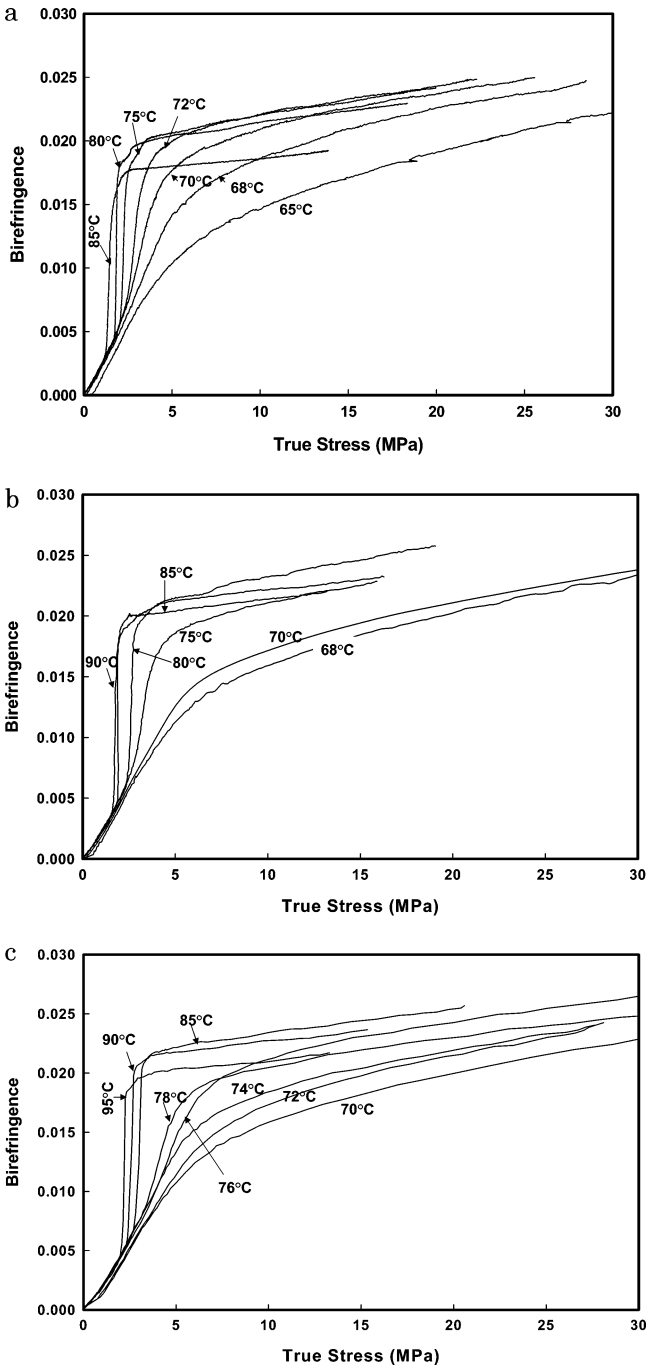

Figure 3. (a) True stress−birefringence plots for PLA films stretched at 60%/min and at various temperatures. (b) True stress−birefringence plots for PLA films stretched at 240%/min and at various temperatures. (c) True stress−birefringence plots for PLA films stretched at 960%/min and at various temperatures.

II decrease with increasing temperature. At higher levels of deformation, deviation from this "regime II" occurs, with birefringence increasing considerably more slowly than stress in "regime IIIc".

Although the traditional stress optical constant is invariant with respect to the rate and temperature of stretching in the range investigated, the data in Figure 3a−c clearly show that the nonlinear part of the stress optical behavior encompassing regimes II and III as well as transitions between I, II, and IIIc are very much dependent on these key processing variables.

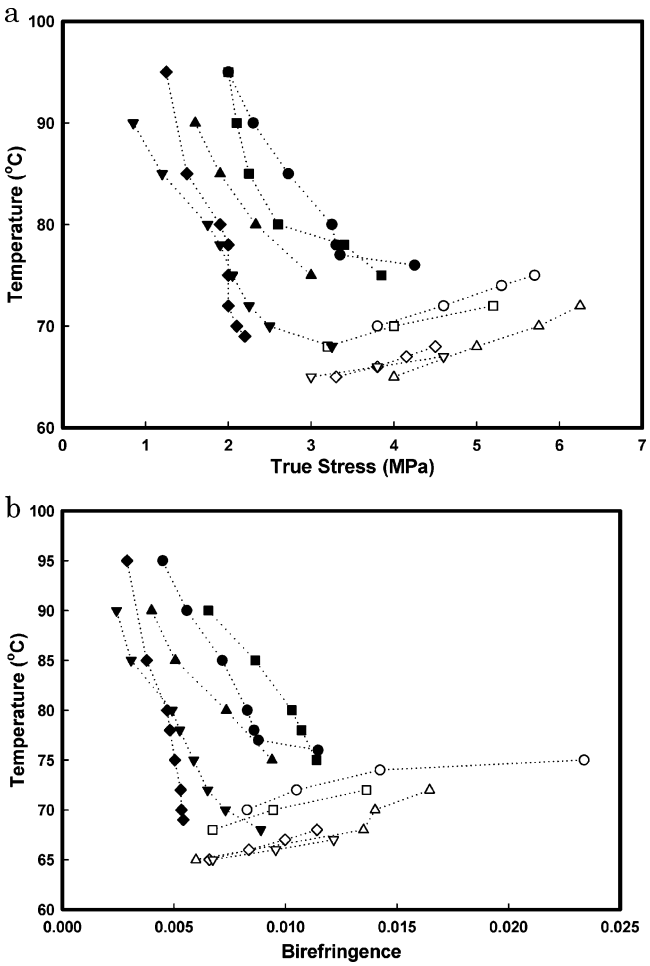

Figure 4. Plots of the true stress (a) and birefringence (b) at phase transition points for films deformed under various conditions. The filled symbols refer to positive deviation (stress-induced crystallization), and the empty symbols refer to negative deviation (nematic-like structure): ●, 960; ■, 480; ▲, 240; ◆, 120; ▼, 60%/min.

The regime II and regime III slopes are plotted as a function of temperature in Figures 5 and 6. The regime II slope tends to increase with decreasing rate and increasing temperature. The regime III stress optical constant tends to decrease with increasing temperature.

To ascertain the structural mechanisms responsible for regimes I, II, and III, we concentrated on the temperature regions where these birefringence−stress curves change from I + IIIa (72 °C) to I + II + IIIc (76 and 78 °C) regime behavior at the temperature range 72−78 °C.

Regime I + IIIa Behavior. During the stretching of the PLA films at temperatures 72 °C and below at a stretching rate of 960%/min, the condition of regime I + IIIa behavior is observed. This condition is characterized by adherence to linear regime I stress optical rule behavior in the early stages of deformation giving way to regime IIIa behavior beyond a critical stress as shown in Figure 7. The off-line WAXD patterns of samples rapidly frozen at various stages of deformation are shown along with the birefringence−true stress plot in Figure 7.

In regime I, the WAXD patterns exhibit the slow development of amorphous chain orientation that manifests itself as gradual concentration of the amorphous

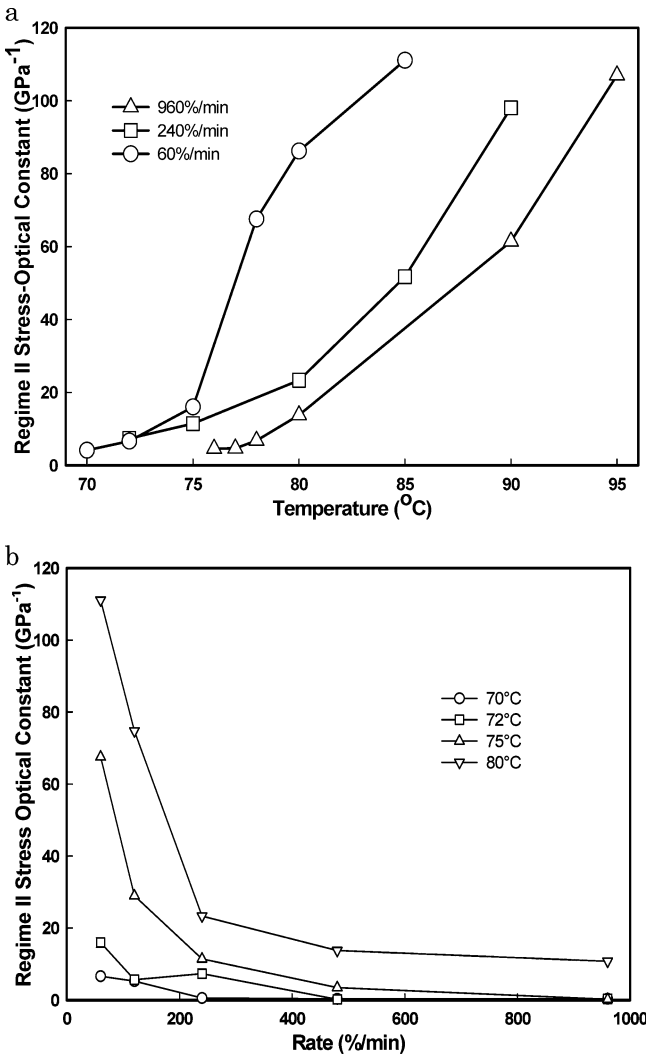

Figure 5. (a) Temperature dependence of the regime II stress−optical relationship slope for PLA films stretched for three different deformation rates. (b) Stretching rate dependence of the regime II stress−optical relationship slope for selected stretching temperatures.

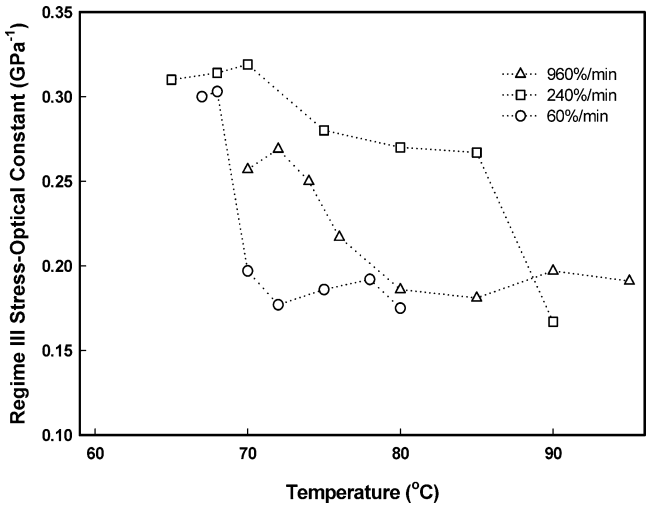

Figure 6. Plot of the regime III stress−optical relationship slope for PLA films stretched under various conditions.

halo in the equatorial direction. At the transition from regime I to regime IIIa, the WAXD intensity rapidly concentrates at the equator, and with further stretching this concentration of intensity continues until the

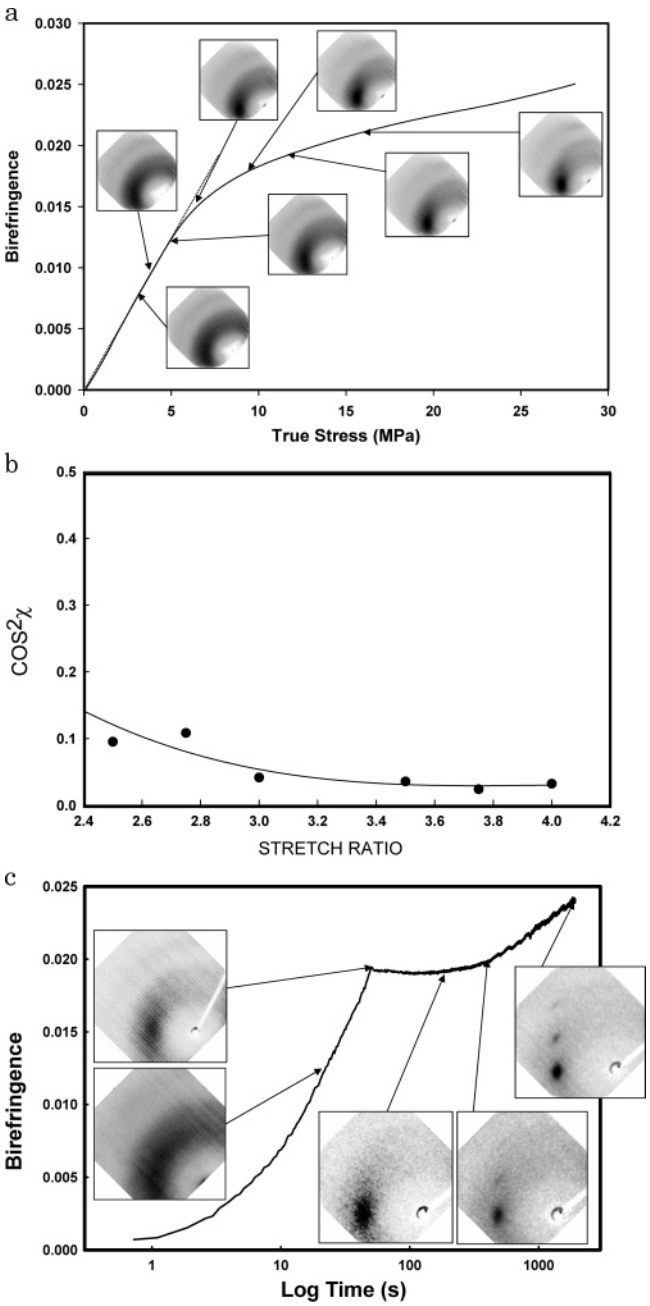

Figure 7. (a) Birefringence−true stress plot for a PLA film stretched to SR 5 at a rate of 960%/min and a temperature of 72 °C with the WAXD images of samples taken at various stages of deformation. (b) Cos^2 χ for the equatorial peak at $2\theta \sim 16°$ as a function of the stretch ratio for PLA films stretched up to SR 5 at a rate of 960%/min and a temperature of 72 °C. (c) Temporal evolution of birefringence in PLA films stretched to 5× stretch ratio at 75 °C and a rate of 500%/min and then maintained at final stretched state at this temperature for a series of holding times.

WAXD patterns exhibit nematic-like order at the highest stretching levels. This is quantitatively depicted by the $\langle \cos^2 \chi \rangle$ values, obtained from the diffraction spot at $2\theta \sim 18°$ that represents the interchain correlation, plotted as a function of deformation level (Figure 7b). These WAXD patterns resemble the results seen previously for nematic liquid crystals,[38−41] indicating that the polymer chains are well oriented in the stretching direction but that the three-dimensional crystalline order is absent as evidenced by the absence of equatorial as well as off-equatorial crystalline diffraction spots. A

most remarkable behavior of this I + IIIa condition is that even at high deformation levels we do not observe any sign of stress-induced crystallization.

This processing temperature is 12 °C above the glass transition temperature, and the chain relaxation processes at this temperature are highly suppressed, particularly when the high deformation rates are employed. As a result, some relaxation may occur during the transportation of the samples to the X-ray machine. However, it does not alter the "character" of the overall structure even though it may alter the "magnitude" of the anisotropy in all of the series of samples that were stretched and exhibit "nematic-like" order. Were the relaxation process to become significant enough to alter this structure, then we would observe this nematic order to convert to strain-induced crystalline structure.

To show this sluggishness in structural conversion, we performed a time evolution study under a typical condition where nematic structure is observed. This is illustrated in Figure 7c. In this experiment, a birefringence vs time curve is developed for a series of samples stretched under identical conditions at 75 °C and 500%/min up to a 5× stretch ratio followed by holding in the clamps at the processing temperature in a series of holding times to simulate the prolonging of relaxation effects. Following their specified holding times at the processing temperature, the samples were quenched to room temperature below the glass transition temperature and then removed from the clamps, and the WAXD patterns were obtained. It is clearly observed that when the stretched films are not held in the clamps, but are cooled immediately following the end of stretching, and then removed from the clamps, the nematic-like order is present. The first evidence of strain-induced crystalline structure is not noticed until after 5 min of holding, which is an extremely long time. This clearly shows that the nematic structures that are exhibited by the PLA are quite stable. Therefore, the off-line WAXD data obtained on samples rapidly quenched, then removed from the clamps, without holding reasonably represent the state of the structure at the end of the stretching.

This nematic order has previously been observed: first by Bonart[42] and then by others through synchrotron studies in PET[43,44] and other polyesters[45] during stretching from amorphous precursors. This structural state is difficult to preserve at the end of stretching as the plastic deformation induced near adiabatic heating typical at high deformation rates coupled with the naturally relatively short PET chains lead to rapid relaxation that takes place when the deformation is stopped. This facilitates crystallization after the completion of stretching as the oriented chains rapidly rearrange into a lattice structure with the added relaxation similar to the experiments shown in Figure 7c. We also do observe this crystallization after the completion of stretching, but at much longer time scales as the PLA chains are substantially longer and entanglement network is substantially denser than PET.

This shows that the WAXD patterns obtained through rapid freezing within the clamps at selected conditions in this research are generally representative of the change in the phase behavior during deformation.

Regime I + II + IIIc Behavior. With a slight increase of temperature from 72 to 76 °C the birefringence−true stress curve changes its character abruptly as illustrated in Figures 8 and 9 (78 °C). Beyond regime I, we observe a positive deviation of slope (in relation to the dotted line extension of SOR regime) marking the transition from regime I to regime II; this gives way to regime IIIc behavior with further stretching. The off-line WAXD patterns taken for various samples are shown along with the birefringence−true stress plot in Figure 8; the points at which these samples were stretched to prior to quenching are indicated with arrows drawn from the WAXD images to the birefringence−true stress plot. The WAXD images clearly show that at the end of the regime I moderate levels of orientation in the amorphous state develop, and beyond this point, positive deviation into regime II accompanies the appearance of highly oriented crystalline diffraction spots. If the relaxation-influenced changes were to have occurred in the transit between stretching and the WAXD measurements, we should have seen the early start of strain crystallization within regime I. The fact that we do not see this attests to the fact that the freezing process employed in this research is quite effective in minimizing the latter effect. Beyond this point, little or no enhancement of the orientation in the crystalline regions is detected, as the azimuthal distribution of intensity in these peaks does not change. This behavior continues until well into the large deformation levels in regime IIIc. This positive deviation from the stress optical rule (regime I−II behavior) has previously

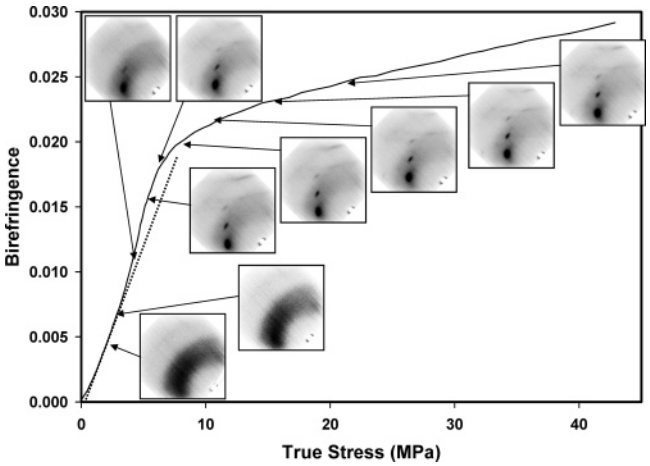

Figure 8. Birefringence−true stress plot for a PLA film stretched to SR 5 at a rate of 960%/min and a temperature of 76 °C with the WAXD images of samples taken at various stages of stretching.

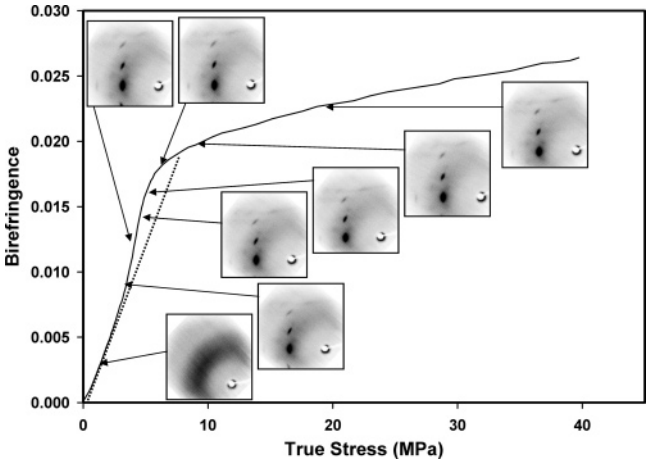

Figure 9. Birefringence−true stress plot for a PLA film stretched to SR 5 at a rate of 960%/min and a temperature of 78 °C with the WAXD images of samples taken at various stages of stretching.

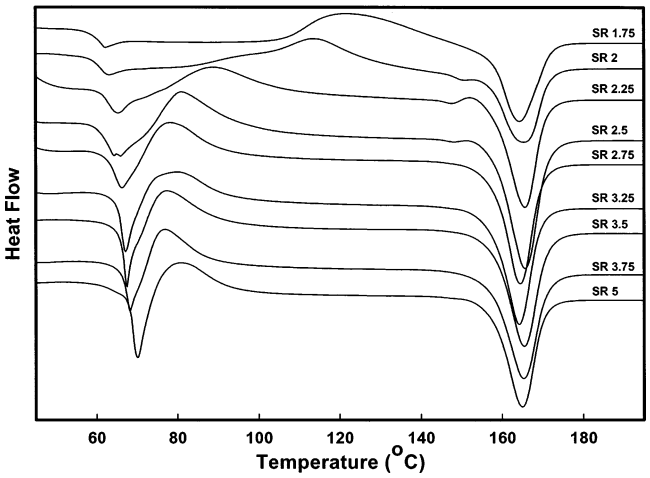

Figure 10. DSC scans for PLA films stretched at a rate of 960%/min at 72 °C.

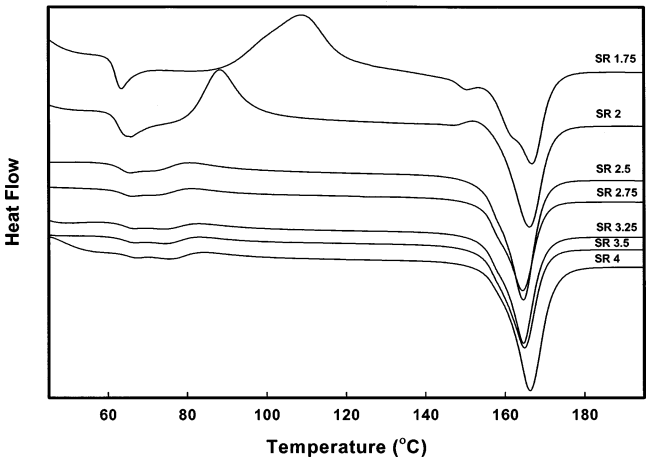

Figure 11. DSC scans for PLA films stretched at a rate of 960%/min at 78 °C.

been observed by Treloar, who showed that crystallization during deformation of natural rubber leads to a positive deviation from the stress optical rule.[14] At 78 °C this positive deviation of birefringence from regime I to regime II becomes more pronounced as illustrated in Figure 9.

The DSC scans of PLA films deformed at 960%/min and 72 °C (regime I + IIIa) and at 78 °C (regime I +II + IIIc) at various stages of deformation are shown in Figures 10 and 11, respectively.

As the film is stretched, the glass transition temperature increases, indicating that the chains become well-packed and less mobile as they become aligned in the stretching direction. The cold crystallization peak becomes sharper and shifts to lower temperature, reflecting the decrease in entropy due to an increased orientation in the amorphous regions as the deformation proceeds. These data are quantitatively shown in Figure 12a,b. Also, crystallinity increases with deformation at 78 °C and reaches a plateau at a point corresponding to the deviation into regime IIIc deformation behavior (Figure 12c).

Strain Optical Behavior. Figures 13 and 14 show the large deformation strain optical behavior of samples stretched in the 65−90 °C range at rates of 60%/min and 960%/min. Within the temperature range from 60 to 70 °C, substantial portions of these curves are linear beyond the initial nonlinear transition. In all cases the slope of the initial nonlinear and secondary linear portion the slope decreases with increasing temperature. The data also indicate that this decrease in the slope of the linear region accelerates around 72 °C while the strain range over which this linearity is observed steadily decreases with the increase of temperature. At this temperature we also observe an abrupt change in the nonlinear optical behavior with the appearance of steeper slope at higher strains. The critical transition points between regimes I and II for strain-crystallized films or between regimes I and IIIa for nematic ordered films identified from the true stress−birefringence plots are shown with small circles and small squares, respectively, on each figure for cross-comparison of the complete mechanooptical behavior.

At all rates the apparent demarcation from linearity corresponds to approximately 1.2 times the T_g of PLA. Although this field has been rather controversial in the past several decades, this transition is strikingly close to the T_{ll} (liquid−liquid transition) expected by Boyer and others ($T_{ll} \sim 1.2T_g$).[46,47] As they amply discussed in the literature, for definitive confirmation, a minimum of three independent techniques (e.g., NMR, DSC, DMA, etc.) are necessary, and we do not have them in this paper. However, if we assume that this transition temperature is correct and real for PLA, the large deformation mechanooptical behavior we present here certainly follows at least certain structural and dynamic aspects of this concept. According to this concept, the amorphous chains exhibit segmental correlations between T_g and T_{ll}, and beyond the T_{ll}, "segmental melting"[48] takes place. It is possible that these segmental correlations enhance the network connectivity while greatly suppressing the relaxation during deformation leading to the observed linear strain optical behavior due to affine-like deformation. The data at these two rates demonstrate that as soon as these preexisting "segmental crystals" disintegrate by the combined effects of higher temperature and slower rates, the relationship becomes nonlinear as the relaxation effects suddenly become pronounced. A remarkable feature of these two strain optical graphs is the fact that, under the conditions where the material remains nematically ordered, the linear portion of the strain optical behavior expands, whereas in those conditions where strain crystallization occurs (higher temperatures and/or lower rates) a highly nonlinear large deformation behavior is observed. The slope at these higher levels of deformation is so large that the plots cross over the data taken at low temperatures and/or fast rates. These evidences suggest that the development of crystallites substantially enhances the long-range connected network that autocatalytically accelerates orientation and further oriented crystallization. Whereas under conditions where the nematic ordered structure is formed (lower temperatures and/or higher rates) the long-range tightly connected network is poorly formed, if it is formed at all, and hence the expansion of the linear or near-linear strain optical behavior to much larger strains. We should also point out that, under the conditions where the nematic-like order is observed, the films were found to be stretched to substantially larger deformation levels without fracture, whereas if the strain-induced crystals form during deformation, the large deformation drawability becomes limited, as can be deduced from their differences in their mechanooptical behavior presented above.

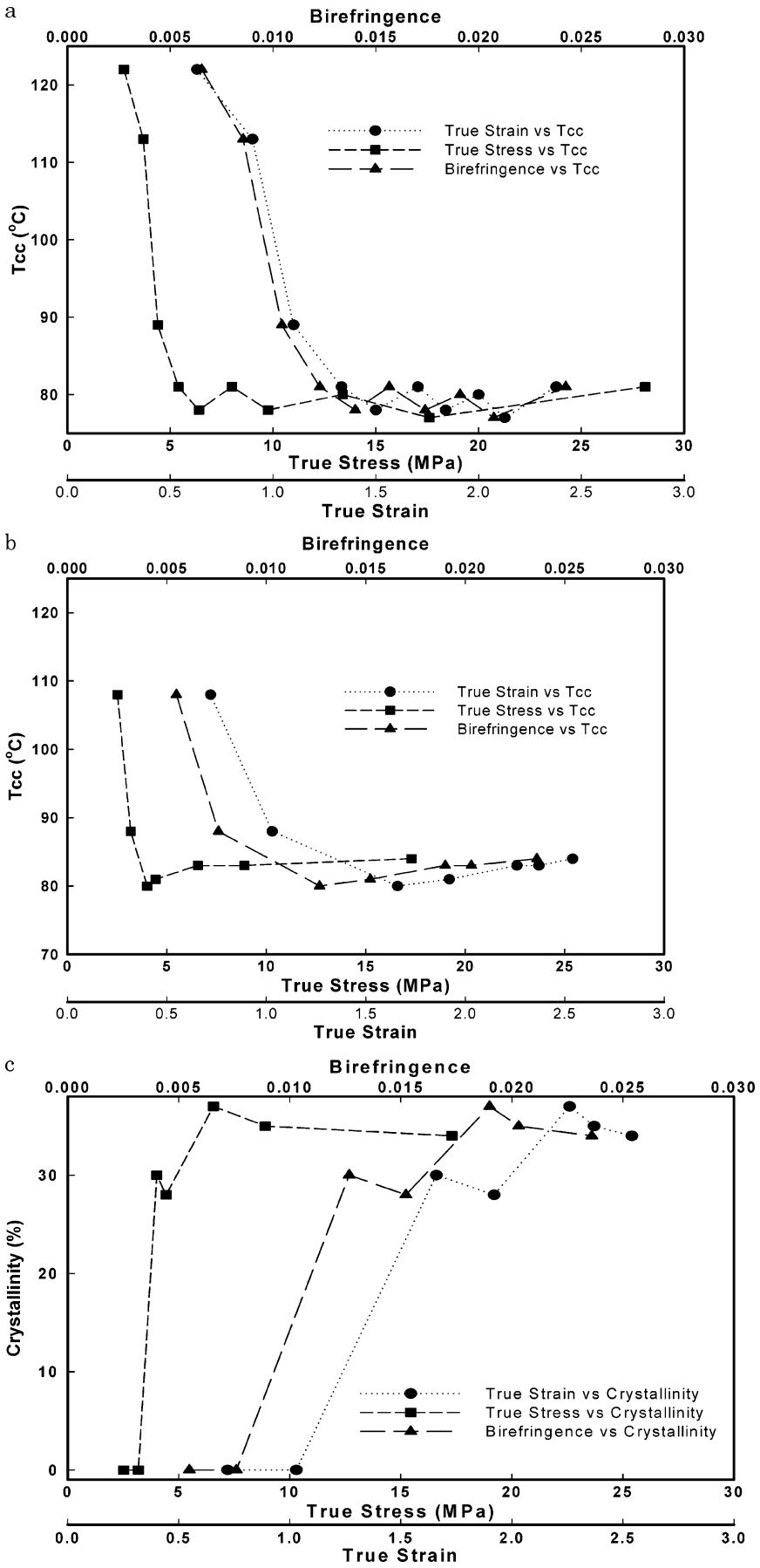

Figure 12. (a) Tcc as a function of the true stress, true strain, and birefringence for PLA films stretched at 960%/min and 72 °C. (b) Tcc as a function of the true stress, true strain, and birefringence for PLA films stretched at 960%/min and 78 °C. (c) Crystallinity Tcc as a function of the true stress, true strain, and birefringence for PLA films stretched at 960%/min and 78 °C.

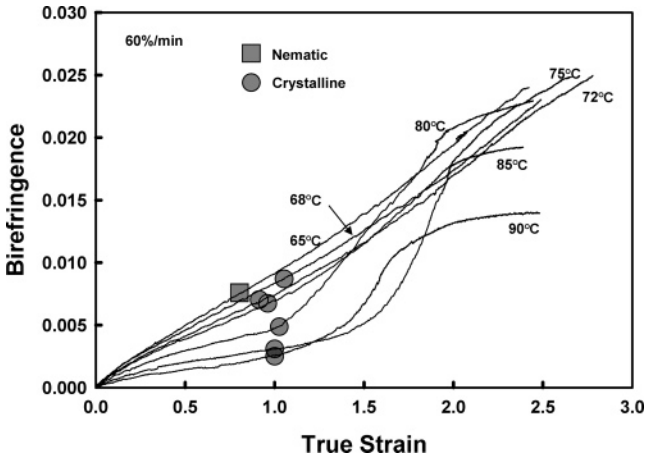

Figure 13. Birefringence−true strain behavior of PLA films stretched at 60%/min. The small squares indicate nematic transitions, and the small circles indicate crystalline transitions.

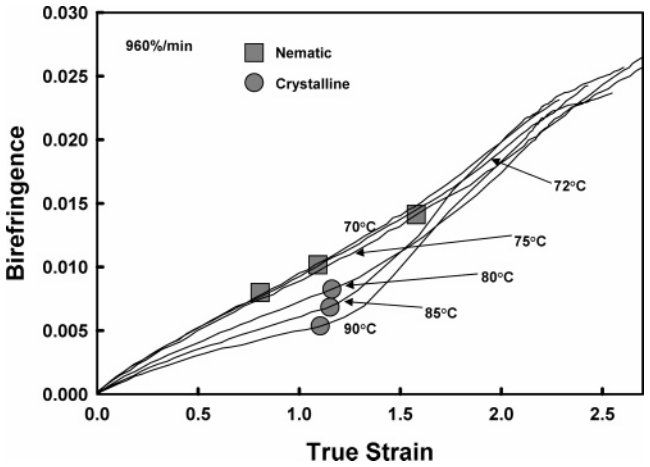

Figure 14. Birefringence−true strain behavior of PLA films stretched at 960%/min. The small squares indicate nematic transitions, and the small circles indicate crystalline transitions.

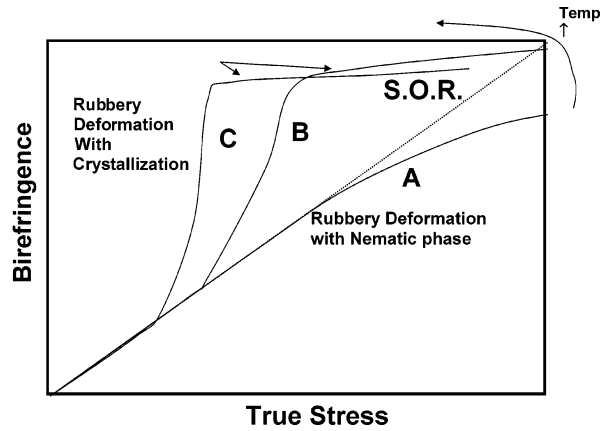

Figure 15. Generalized behavior for the deformation of slow crystallizing materials.

Structural Interpretation

The generalized stress optical behavior for slow crystallizing materials is shown in Figure 15. Curve A represents the behavior of a film deformed at relatively high rates and at relatively low temperatures. The material adheres to regime I stress optical rule behavior during the early stages of deformation; this is followed by negative deviation from linearity into regime IIIa associated with the polymer chains nearing their finite extensibility. The deviation from regime I linearity is negative in nature for samples stretched at higher rates and lower temperatures, with higher rates and lower temperatures favoring earlier deviation from linearity. This negative deviation is similar to that described by Inoue et al.[17−23] Here, crystallization does not cause the deviation from regime I stress optical rule behavior, but the deviation is due to the non-Gaussian segmental distribution characteristic of polymer chains as they approach their finite extensibility.

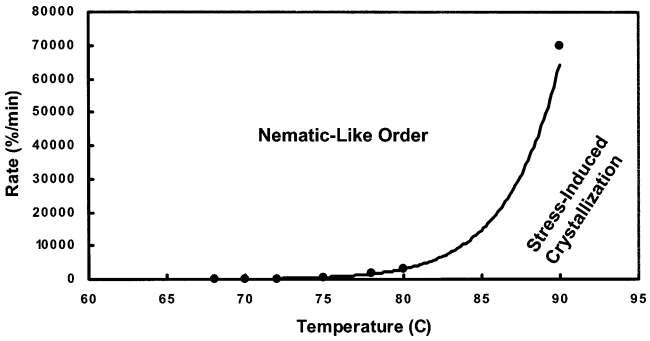

Figure 16. Phase diagram for for structure formation during the uniaxial deformation of PLA.

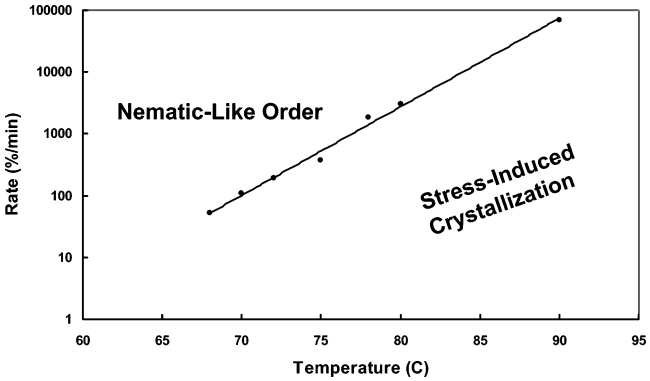

Figure 17. Phase diagram for structure formation during the uniaxial deformation of PLA with logarithmic scale for rate.

As the temperature is increased and/or the deformation rate is decreased, the material approaches the behavior exhibited by curves B and C. Curves B and C possess the same initial stress optical rule behavior (same stress optical constant) seen in curve A but exhibit positive deviation from regime I into regime II. This is likely due to the higher propensity for crystallization to occur under these conditions. The higher temperatures obviously enhance crystallization by inducing partial local relaxation of the chains, thereby allowing them to register with each other, establishing the crystalline network. In turn, this leads to a faster increase in birefringence over a small range of stress. The deformation at low rates tends to cause a slower increase in stress and likely enhances crystallizability due to the longer stretching times, allowing "thermally assisted" strain-induced crystallization to occur. This is very similar to rapid formation of physical cross-links, manifesting here in the form of crystalline domains containing polymer chains that exhibit near perfect orientation as evidenced by the WAXD measurements. This orientation does not change with further deformation. Under these conditions, the material shows a negative deviation from regime II into regime IIIc due

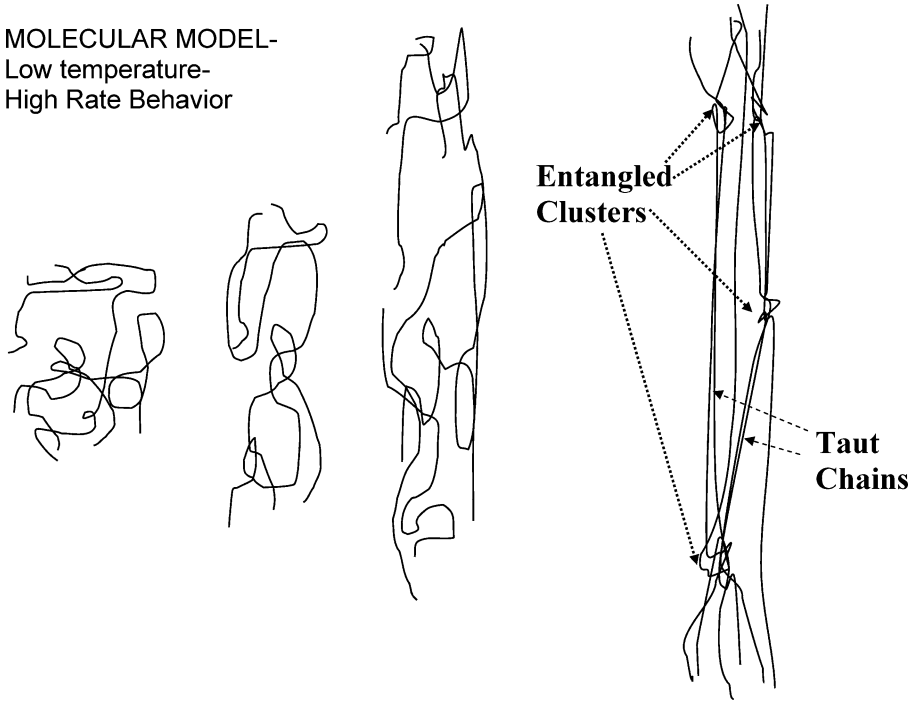

Figure 18. Molecular model of deformation in the rubbery state at relatively low temperatures (ca. T_g to $T_g + 10$) and at sufficiently high rates (arrows indicate locations of the nematic ordered regions exhibiting near perfect orientation spanning the regions between the entangled clusters).

to the resistance caused by the increased density of this crystalline physical network, preventing further orientation of the polymer chains. There are also additional evidences as to the dynamics of the overall structural formation by examining the slope of each regime. We have observed that in the samples exhibiting regime I + II + III behavior the slope of the regime IIIc is lower than that of regime IIIa in those samples showing only the regime I + III behavior. Obviously, this shows that in the absence of crystalline "nodes" the samples exhibiting regime I + III behavior do not have a "locked-in" structure, and they continue to deform upon stretching in regime IIIa with the observed changes in the birefringence.

In the samples exhibiting regime I + II + IIIc behavior, the regime IIIc stress optical constant is lower at higher temperatures due to the higher density of the crystalline network, and the polymer chains become locked in their orientation, leading to the observed lower increases in birefringence with increasing stress. The large deformation strain optical behavior indicates that at temperatures between T_g and $1.2T_g$ (which has been defined as T_{ll}) segmental correlations lead to large linear strain optical behavior associated with the formation of nematic like order. Beyond this temperature range the "segmental correlations" present in the amorphous film "melt", and a largely nonlinear strain optical behavior is observed. This behavior accompanies strain-induced crystallization.

Dynamic Phase Diagram

The data in Figure 5b for the regime II SOC at various temperatures as a function of rate were fit to the power law function:

$$y = Kx^n$$

where y is the regime II SOC, x is the temperature, K is the power law coefficient, and n is the power law index.

After determining the power law fit, the point at which the regime II SOC becomes that of the regime I SOC (i.e., when regime II first disappears) was taken as the demarcation between regime I + II + IIIc behavior and regime I + IIIa. This was used to develop the quantitative phase diagram for the structure formation during the uniaxial deformation of PLA films in the rubbery state as shown in Figures 16 and 17. The phase diagram shows that low temperatures and high rates favor the formation of a nematic-like phase during deformation, while high temperatures and low rates favor crystallization while deformation proceeds. As the temperature increases, the rate at the transition increases exponentially as implied in the semilog representation shown in Figure 17.

Molecular Model

Figures 18 and 19 show conceptual molecular models for the uniaxial deformation of slow crystallizing materials at relatively low temperatures and high rates (Figure 18) and at relatively high temperatures and low rates (Figure 19). At low temperatures and/or high rates, the polymer chains begin to orient during the early stages of deformation. As the deformation proceeds, the polymer chains become well-oriented, and they begin to approach their finite extensibility with little or no relaxation playing a role in the process. We believe the main reason that the polymer chains do not crystallize is due to the lack of adequate relaxation that would have facilitated the registry of highly oriented adjacent chains to form crystalline lattice. This is in accord with some of the recent molecular dynamics simulations on the deformation of polymer chains where entangled chain clusters were shown to connect to each other with taut chains that are not necessarily parallel to each other.[49] Instead, they remain in the highly

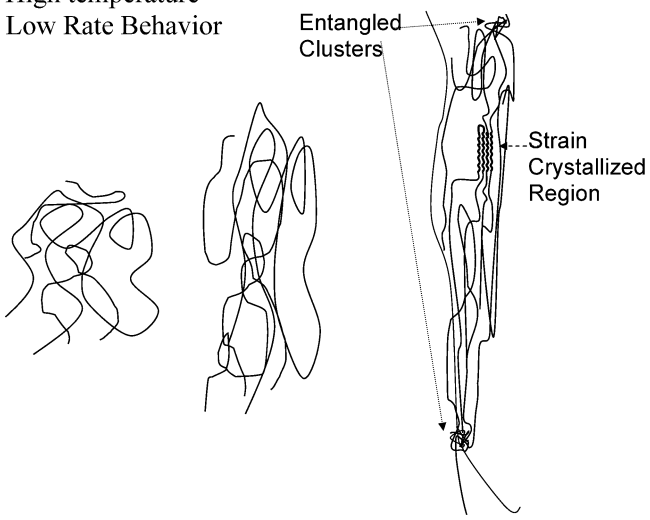

Figure 19. Molecular model of the deformation in the rubbery state at relatively high temperatures (ca. T_g + 10 to Tcc) and at sufficiently low rates.

oriented state with nematic like order and the accompanying substantial translational and minor splaying disorder of chain axes (Figure 18).

At high temperatures and/or low rates, after enough time (at low rates) or with enough thermal energy (at high temperatures), the polymer chains at intermediate levels of orientation strain crystallize. The formation the network consisting of crystallite nodes and entanglement junctions causes an autocatalytic rapid rise in oriented crystallization. In this mode, the crystallization is promoted by a sufficient amount of relaxation that occurs as part of the deformation (Figure 19).

Conclusions

We characterized the effect of temperature and stretching rate on the linear and nonlinear stress optical behavior of poly(L-lactic acid). At higher temperature and/or lower rates we observed three regimes of stress optical behavior during the rubbery state deformation of PLA: regime I is characterized by SOR behavior, regime II is characterized by a rapid increase in birefringence due to formation of long-range network whose nodes are rapidly increased with crystallization, and regime IIIc is characterized by slow increase in birefringence due to non-Gaussian behavior. At lower temperatures and higher rates we observed a two-regime behavior with the first regime following the linear stress optical rule while the material remains amorphous. In the regime IIIa, a negative deviation from stress optical rule is observed and at all large deformation levels, and the structure possesses a "nematic-like" order. This phase forms due to the lack of adequate chain relaxation during deformation in this polymer that results from PLA containing relatively high chain entanglement densities. The nature of the strain optical behavior was found to depend on the phase that develops during deformation. If the nematic-like order is formed, a large linear or near-linear strain optical behavior is observed. Under the conditions where the strain-induced crystallization forms, the strain optical behavior becomes highly nonlinear. A quantitative dynamic phase diagram and molecular model for the structure formed during the deformation of PLA is presented. These may be extended to other slow crystallizing polymers.

Acknowledgment. Financial support for this research was provided by United States Department of Agriculture Grant 99-355-04-7823. The authors gratefully acknowledge the material (Natureworks 4043D) provided by Cargill Dow LLC Corp.

Note Added after ASAP Posting. Labels in Figures 2, 3, and 17 were changed in the version posted ASAP February 9, 2005; the corrected version was posted February 22, 2005.

References and Notes

(1) Lam, K. H.; Nijenhuis, A. J.; Bartels, H.; Postema, A. R.; Jonkman, M. F.; Pennings, A. J.; Nieuwenhuis, P. *J. Appl. Biomater.* **1995**, *6*, 191−197.
(2) Heino, A.; Naukkarinen, A.; Kulju, T.; Toermaelae, P.; Pohjonen, T.; Maekelae, E. A. *J. Biomed. Mater. Res.* **1996**, *30*, 187−192.
(3) Gruber, P. R.; Hall, E. S.; Kolstad, J. J.; Iwen, M. L.; Benson, R. D.; Borchardt, R. L. U.S. Pat. 5,247,073, 2001.
(4) Sen, T. Z.; Toki, S.; Cakmak, M. *SPE ANTEC* **2001**, *59*, 1510−1514.
(5) Lee, S. W.; Cakmak, M. *J. Macromol. Sci., Phys.* **1998**, *B37*, 501−526.
(6) Galay, J.; Cakmak, M. *J. Polym. Sci., Part B: Polym. Phys.* **2001**, *39*, 1107−1121.
(7) Kim, J. C.; Cakmak, M.; Zhou, X. *Polymer* **1998**, *39*, 4225−4234.
(8) Kokturk, G.; Serhatkulu, T. F.; Cakmak, M.; Piskin, E. *Polym. Eng. Sci.* **2002**, *42*, 1619−1628.
(9) Hopper, M.; Martin, M. Eur. Pat. Appl. 81926, 1983; p 9.
(10) Song, S. S.; White, J. L.; Cakmak, M. *Polym. Eng. Sci.* **1990**, *30*, 944−949.
(11) Janeschitz-Kriegl, H. In *Polymer Melt Rheology and Flow Birefringence*; Springer-Verlag: Berlin, 1983; p 522.
(12) Reiss-Nunes, R. C.; Riande, E.; Guzman, J.; Chavez, N. A. *Macromolecules* **2000**, *33*, 9464−9467.
(13) Salem, D. R. *Polymer* **1992**, *33*, 3182−3188.
(14) Treloar, L. R. G. In *Physics of Rubbery Elasticity*, 2nd ed.; Clarendon: Oxford, 1958; p 342.
(15) Stein, R. S. *Polym. Eng. Sci.* **1976**, *16*, 152−157.
(16) Matsumoto, T.; Bogue, D. C. *J. Polym. Sci., Phys.* **1977**, *15*, 1663−1674.
(17) Ryu, D. S.; Inoue, T.; Osaki, K. *Polymer* **1998**, *39*, 2515−2520.
(18) Inoue, T.; Ryu, D. S.; Osaki, K.; Takebe, T. *J. Polym. Sci., Part B: Polym. Phys.* **1999**, *37*, 399−404.
(19) Inoue, T.; Okamoto, H.; Osaki, K. *Macromolecules* **1991**, *24*, 5670−5675.
(20) Inoue, T.; Osaki, K. *Macromolecules* **1996**, *29*, 1595−1599.
(21) Osaki, K.; Okamoto, H.; Inoue, T.; Hwang, E. *Macromolecules* **1995**, *28*, 3625−3630.
(22) Okamoto, H.; Inoue, T.; Osaki, K. *Macromolecules* **1992**, *25*, 3413−3415.
(23) Inoue, T.; Okamoto, H.; Osaki, K. *Macromolecules* **1992**, *25*, 7069−7070.
(24) Inoue, T.; Ryu, D. S.; Osaki, K. *Macromolecules* **1998**, *31*, 6977−6983.
(25) Kroeger, M.; Luap, C.; Muller, R. *Macromolecules* **1997**, *30*, 526−539.
(26) Subramanian, P. R.; Galiatsatos, V. *Makromol. Chem., Macromol. Symp.* **1993**, *76*, 233−240.
(27) Muller, R.; Froelich, D. *Polymer* **1985**, *26*, 1477−1482.
(28) Muller, R.; Pesce, J. J. *Polymer* **1994**, *35*, 734−739.
(29) Welsh, G. E.; Blundell, D. J.; Windle, A. H. *J. Mater. Sci.* **2000**, *35*, 5225−5240.
(30) Blundell, D. J.; Mahendrasingam, A.; Martin, C.; Fuller, W. *J. Mater. Sci.* **2000**, *35*, 5057−5063.
(31) Welsh, G. E.; Blundell, D. J.; Windle, A. H. *Macromolecules* **1998**, *31*, 7562−7565.
(32) Mulligan, J.; Cakmak, M. *SPE ANTEC* **2003**, *61*, 1588−1592.
(33) Mulligan, J.; Cakmak, M. *SPE ANTEC* **2003**, *61*, 1593−1596.
(34) Mulligan, J.; Cakmak, M.; Sen, T. Z. *SPE ANTEC* **2002**, *60*, 1646−1650.
(35) Kokturk, G.; Serhatkulu, T. F.; Cakmak, M. *SPE ANTEC* **2000**, *58*, 1737−1741.
(36) Koike, Y.; Cakmak, M. *Polymer* **2003**, *44*, 4249−4260.
(37) Fischer, E. W.; Sterzel, H. J.; Wegner, G. *Kolloid Z. Z. Polym.* **1973**, *251*, 980−990.
(38) Francescangeli, O.; Laus, M.; Galli, G. *Phys. Rev. E* **1997**, *55*, 481−487.

(39) Chang, S.; Han, C. D. *Macromolecules* **1997**, *30*, 1670−1684.
(40) Chang, S.; Han, C. D. *Macromolecules* **1996**, *29*, 2383−2391.
(41) Kim, G. H.; Jin, S.; Pugh, C.; Cheng, S. Z. D. *J. Polym. Sci., Phys* **2001**, *39*, 3029−3037.
(42) Bonart, R. *Kolloid Z. Z. Polym.* **1966**, *213*, 1−11.
(43) Blundell, D. J.; Mackerron, D. H.; Fuller, W.; Mahendrasingam, A.; Martin, C.; Oldman, R. J.; Rule, R. J.; Riekel, C. *Polymer* **1996**, *37*, 3303−3311.
(44) Kawakami, D.; Hsiao, B. S.; Ran, S.; Burger, C.; Fu, B.; Sics, I.; Chu, B.; Kikutani, T. *Polymer* **2004**, *45*, 905−918.
(45) Mahendrasingam, A.; Martin, C.; Fuller, W.; Blundell, D. J.; Oldman, R. J.; MacKerron, D. H.; Harvie, J. L.; Riekel, C. *Polymer* **1999**, *41*, 1217−1221.
(46) Boyer, R. F.; Heesche, J. P.; Gillham, J. K. *J. Polym. Sci., Phys* **1981**, *19*, 13−21.
(47) *Order in the Amorphous State of Polymers*; Keinath, S. E., Miller, R. L., Rieke, J. K., Eds.; Plenum: New York, 1987; p 478.
(48) Lobanov, A. M.; Ya Frenkel, S. *Polym. Sci. USSR* **1980**, *22*, 1150−1163.
(49) Yashiro, Y.; Ito, T.; Tomita, Y. *Int. J. Mech. Sci.* **2003**, *45*, 1863−1876.

MA048794F